Two-Dimensional Penning Ionization Electron Spectroscopy of NNO, HCNO, and HNNN: Electronic Structure and the Interaction Potential with He*(2^3S) Metastable and Li(2^2S) Ground State Atoms

Tibor Pasinszki,*,† Naoki Kishimoto, and Koichi Ohno*

Department of Chemistry, Graduate School of Science, Tohoku University, Aramaki, Aoba-ku, Sendai, 980-8578, Japan

Received: April 28, 1999; In Final Form: June 28, 1999

The electronic structure and Penning ionization of NNO, HCNO, and HNNN upon collision with He*(2^3S) metastable atoms were studied using He I photoelectron and two-dimensional Penning ionization electron spectroscopies (2D-PIES). From the peak shifts in PIES and collision energy dependence of partial Penning ionization cross sections, the interaction potentials between molecules and He*(2^3S) atoms were deduced. In the studied collision energy range, the interaction potential was found to be attractive around the nitrile oxide (−CNO) and azide (−NNN) groups, but no characteristic interaction was observed between NNO and He*(2^3S). Ab initio calculations on the similar interacting systems M−Li(2^2S) (where M = NNO, HCNO, and HNNN) at the CCSD/6-311++G** level revealed fine details of the anisotropy of the interaction potentials and were in good agreement with experimental results. The spectroscopic investigations predicted the existence of thermodynamically stable MLi radicals, and the structure and stability of HCNOLi and HNNNLi were calculated at the QCISD/6-311++G** level.

I. Introduction

Chemical reactions, energy transfer, electron transfer, and molecular collisions between molecules take place through a close intermolecular contact, and they are strongly influenced or governed by the interaction potential between the reacting species; therefore, in order to understand the dynamics and kinetics of intermolecular processes it is important to study and derive information about the latter. Besides various molecular beam experiments, which can partially or fully fulfill this role, kinetic energy resolved Penning spectroscopy is a novel and unique electron spectroscopic technique which provides information directly about the interaction potential between molecules and metastable rare gas atoms. Since the triplet metastable rare gas atom−molecule interaction potential is very similar to those of alkali metal−molecule potentials, the method provides indirect information about these latter chemically important interactions and has a predicting power for the existence and possible structure of stable alkali metal complex radicals.[1] Penning spectroscopy, furthermore, provides information about the exterior regions of the molecules with indicating places for electrophile attack in chemical reactions, because the metastable atoms cannot penetrate into the interior regions of molecules.

In Penning ionization electron spectroscopy (PIES), molecules (M) are collided with metastable rare gas atoms, e.g., He*(2^3S), having higher excitation energy than the ionization potential (IP) of the molecules, and the kinetic energy (E_{ek}) of the ejected electrons (e^-) is analyzed (eq 1).

$$M + He^*(2^3S) \rightarrow M_i^+ + He + e^- \qquad (1)$$

$$E_{ek} = E_{He^*} - IP_i + \Delta E_i$$

$$M + h\nu \rightarrow M_i^+ + e^- \qquad (2)$$

$$E_{ek} = E_{h\nu} - IP_i$$

The technique of PIES is similar to the UV photoelectron spectroscopy (UPS), where the energy of an electron ionized by single photon absorption is measured (eq 2). One of the important differences between PIES and UPS is that the energy difference between the measured electron kinetic energies and the known metastable excitation energy does not provide the IPs, unlike to UPS; thus, there is a small peak energy shift (ΔE_i) if PIES and UPS spectra are compared to each other on an electron energy scale. This peak energy shift depends on the difference between the incoming M + He*(2^3S) (called interaction potential) and outgoing M_i^+ + He potential curves, but assuming a flat potential to the outgoing channel in the ionization region, it is determined by the incoming potential, thus, vice versa, information on the interaction potential can be obtained from the peak energy shifts. In a simplified sense, one can expect that ΔE_i is positive if the interaction is repulsive and negative if the interaction is attractive. In this latter case, the peak shift is the measure of the well depth of the attractive interaction potential. Since there is a similarity between M + He*(2^3S) and M + Li(2^2S) interaction potentials, and given that this latter is the ground state potential of the M−Li system, the large negative peak shift (deep well on the potential surface) in PIES indirectly indicates the existence of thermodynamically stable M−Li radicals. Since PIES bands originate from the ionization of molecular orbitals (MOs), which are more or less localized on a special part of the molecule, the structure or

* Corresponding author. E-mail: ohnok@qpcrkk.chem.tohoku.ac.jp.
† Permanent address: Department of Inorganic Chemistry, Technical University, H-1521 Budapest, Hungary.

10.1021/jp991394n CCC: $18.00
Published on Web 08/10/1999

complexation site of M to Li can also be derived from the PIES spectrum. On the basis of PIES investigations, we predicted, e.g., the existence of CH_3CNLi, and recently this radical was identified in our laboratory in the gas phase by laser evaporation and subsequent reaction of lithium metal with CH_3CN vapors.[2] CH_3CNLi was also identified very recently by P. H. Kasai in solid argon matrix using ESR spectroscopy.[3]

Another characteristic of the Penning ionization process, which can be used to derive information about the interaction potential even if the peak shift is not clearly observed due to broad and/or overlapping bands, is the collision energy dependence of the ionization cross section. The energy of the electron released in the ionization process provides information about the ionic state formed, and electron intensities for respective bands determine the partial ionization cross sections. By measuring the Penning ionization cross section as a function of both the electron energy and metastable atom collision energy (two-dimensional PIES, 2D-PIES), it is possible to obtain not only the dependence of the total ionization cross section but the dependence of the partial ionization cross sections as well. These latter, as ionic states originate from removing an electron from a MO, provide information about the anisotropy of the interaction potential depending on the localization of MOs. One-dimensional cuts from the two-dimensional spectrum give the collision energy dependence of partial ionization cross sections (CEDPICS; ionic state is fixed) and collision energy resolved PIES (CERPIES; metastable atom kinetic energy is constant).

The 2D-PIES method has been recently developed in our laboratory,[4] and in combination with the cross-correlation time-of-flight technique with pseudorandom chopper,[5] it turned out to be a very powerful tool to study the interaction between molecules and metastable atoms. The most important questions we want to answer with a series of studies are the characteristics and anisotropy of the interaction potential, the effect of electronegativity, valence, and bonding of atoms on this, the interaction around chemical groups or bonds, and the influence of substituents on these. Previous CEDPICS[1,6−14] and recent 2D-PIES[15,16] studies on various molecular targets have indicated that the interaction potential is anisotropic between molecules and He*(2^3S) atoms and pointed out the importance of the chemical groups in describing the interaction. It has been observed that the interaction is repulsive around saturated hydrocarbons, alkyl groups, or CH bonds[1,6−10,13,15,16] but attractive around the π region of unsaturated hydrocarbons,[7,8] heterocycles,[10] and C═O double bonds.[8] Studies of alcohols,[9,15] aldehides,[8] ethers,[9,11] amines,[12] isocyanates,[13] nitriles,[1,12,16] and isonitriles[1] have indicated that the interaction is attractive in the lone electron pair region of first-row nonmetal atoms (O, N, and C). There is relatively little known about the molecules containing heavier elements so far, and these studies have focused on organic chlorides and on sulfur compounds in comparison with the oxygen analogue. According to these studies, the interaction potential is attractive around the chlorine atom,[6,14] but in the case of sulfur atom it is strongly depend on the molecular environment; a very attractive potential was found in the sulfur lone pair region in alkyl thioethers and thioalcohols,[15] but no special character (only weakly attractive or weakly repulsive) was detected in the sulfur lone pair region of methyl thiocyanate,[13] methyl isothiocyanate,[13] and thiophene.[10] The interaction potential, with He* or Li, around nitrile oxide (−CNO) and azide (−NNN) functional groups has never been studied before.

In this paper we present a combined experimental (UPS, PIES) and theoretical study of the structure of NNO, HCNO, and HNNN, and the first study of their interaction with He*(2^3S) and Li atoms using 2D-PIES and ab initio calculations. Relevant to this work are the earlier He I photoelectron spectroscopic investigations of NNO,[17,18] HCNO,[19] and HNNN[19−21] and the PIES investigation of NNO.[22,23] Of particular interest are the electronic structure of molecules, the anisotropy of the interaction between molecules and He*(2^3S) or Li(2^2S) atoms, as well as the possible existence, stability, and structure of M−Li inorganic radicals.

SCHEME 1

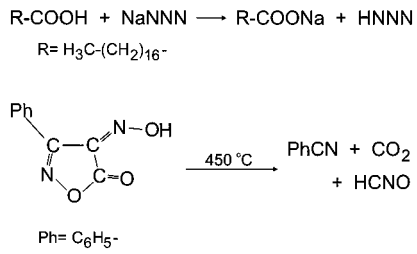

II. Experimental Section

NNO was a commercial product (Showa Denko) and was used without further purification. HCNO[24] and HNNN[25] were synthesized according to literature methods, as briefly described below (see Scheme 1). 3-Phenyl-4-oximino-isoxazol-5-(4H)-one was synthesized by nitrosation of 3-phenyl-5-isoxazolone (Aldrich).[26] NaNNN and stearic acid were commercial products (Nacalai Tesque).

HCNO was synthesized by flush vacuum thermolysis of 3-phenyl-4-oximino-isoxazol-5-(4H)-one.[24] The thermolysis was carried out in a quartz tube (no filling, 12 mm i.d.) heated along 25 cm at 450 °C. The vapors of the precursor were passed through the furnace from a flask held at 110−120 °C. The furnace was directly connected to the spectrometer via two consecutive U-traps. The temperature of the first trap was held around −50 °C to trap phenyl cyanide, and the temperature of the second was so adjusted, by adjusting the distance between the surface of liquid nitrogen in a Dewar-flask and the bottom of the U-trap, that the CO_2 side product could just pass through into the spectrometer; therefore, the formation of CO_2 could be continuously monitored during the generation of HCNO. Essentially pure HCNO was collected in the second trap. Since the vapor pressure of the precursor was low at 110−120 °C, the sample was collected in the course of 14 h; then the trap was separated and the temperature was raised to obtain sufficient vapor pressure for spectroscopic investigations. We observed only trace amounts of the isomer HNCO, which was pumped off at low temperature. (HNCO was slightly more volatile than HCNO.)

HNNN was synthesized by solid−liquid reaction between sodium azide and molten stearic acid.[25] NaNNN and solid stearic acid were mixed at room temperature, placed into a flask, which was connected directly to the spectrometer via a U-trap, and gradually warmed above the melting point of the acid to obtain a fast continuous bubbling of the gaseous products. The volatiles, which was essentially pure HNNN, were condensed in the U-trap with liquid nitrogen; only trace amounts of CO_2 and N_2 were detected. The temperature of the trap was than increased to obtain sufficient vapor pressure for the spectroscopic investigations. With this method, we could produce 1−2 mL of pure liquid HNNN in 20−30 min and did not experience any problem with handling the potentially explosive HNNN at low temperatures.

The instrument used in this work for recording the UPS, PIES, and 2D-PIES spectra was reported in previous papers.[4,6,7,27] UPS spectra were measured by utilizing the He I resonance line (21.22 eV) produced by a pure helium discharge. Metastable atoms for PIES were produced by a negative discharge nozzle source, and the He*(2^1S) component of the He*(2^1S,2^3S) beam was quenched by a water-cooled helium discharge lamp. The kinetic energies of electrons ejected by photo or Penning ionization were determined by a hemispherical electrostatic deflection type analyzer using an electron collection angle of 90° to the incident photon or He*(2^3S) beam axis. The energy resolution of the electron analyzer was 50 meV, estimated from the full width at half-maximum (fwhm) of the $Ar^+(^2P_{3/2})$ peak in the He I UPS spectrum. The transmission of the electron energy analyzer was determined by comparing our UPS data of O_2, CO, N_2, and some hydrocarbons with those of Gardner and Samson[28] and Kimura et al.[18]

In the collision energy resolved experiments, 2D-PIES, the metastable atom beam was pulsed by a pseudorandom chopper and introduced into the reaction cell located 504 mm downstream from the chopper disk. As reference, the intensities of metastable atoms were determined by inserting a stainless steel plate into the reaction cell and measuring the intensity of secondary electrons emitted. The resolution of the electron energy analyzer was lowered to 250 meV (fwhm for He I UPS of Ar) in order to gain higher electron counting rates. Thus, in these experiments, the intensity of emitted electrons from sample molecules (I_e) or from a reference stainless steel plate (I_{He*}) was measured as a function of electron kinetic energy (E_{ek}) and time (τ). Electron energies were scanned by 35 meV steps, and a dwell time for the time-dependent measurement was 3 μs. The 2D electron intensity spectra, $I(E_{ek},\tau)$, were then converted sequentially to $I(E_{ek},\tau_{TOF})$ and $I(E_{ek},\nu_{He*})$ (where τ_{TOF} is the time-of-flight and ν_{He*} is the velocity of the metastable atoms). The 2D Penning ionization cross sections $\sigma(E_{ek},\nu_r)$ were obtained from $I(E_{ek},\nu_{He*})$ using eqs 3 and 4, and finally $\sigma(E_{ek},\nu_r)$ was converted to the 2D-PIES, $\sigma(E_{ek},E_c)$ using eq 5.

$$\sigma(E_{ek},\nu_r) = c[I_e(E_{ek},\nu_{He*})/I_{He*}(\nu_{He*})](\nu_{He*}/\nu_r) \quad (3)$$

$$\nu_r = [{\nu_{He*}}^2 + 3kT/M]^{1/2} \quad (4)$$

$$E_c = \mu\nu_r^2/2 \quad (5)$$

where c, ν_r, k, T, M, and μ are a constant, the relative velocity of metastable atoms averaged over the velocity of the target molecule, the Boltzmann constant, the gas temperature, the mass of the target molecule, and the reduced mass of the system, respectively.

III. Calculations

To assist with experimental data, the interaction potential between target molecules (M) and metastable He*(2^3S) atoms was modeled by approximating the M−He*(2^3S) surfaces with those of M−Li(2^2S). Using this widely accepted approximation, based, e.g., on cross-scattering experiments indicating very similar shape for the velocity dependence of the total scattering cross section and for the location and depth of the well of the attractive interaction potential for He*(2^3S) and Li(2^2S) with various atomic and molecular targets,[29] all of the difficulties could be bypassed that would be associated with calculating the excited-state M−He* surfaces. Thus, the M−Li(2^2S) interaction potentials, $V^*(R,\theta)$ (where R is the distance from the center of mass (X) of the molecule, and θ is the Li−X−O or Li−X−N(3) angle) were calculated by pulling the Li atom toward the center of mass of the molecules and keeping the molecular geometries fixed at the experimental values determined from microwave spectroscopic data;[30] this latter assumption meant that the geometry relaxation by the approach of the metastable atom was negligible in the ionization process. All calculations for the interaction potential were done at the CCSD-(fc)/6-311++G** level of theory, and the full counterpoise (CP) method[31] was used to correct for the basis set superposition errors (BSSE).

The structures of HCNOLi and HNNNLi inorganic radicals were fully optimized at the QCISD(fc)/6-311++G** level of theory, taking advantage of analytic first derivatives at this level in Gaussian-94, and then harmonic vibrational frequencies were calculated at the equilibrium geometries using numeric second derivatives to make sure they were real minima on the potential energy surface. In the frequency calculations, divergency problems in the post-HF iteration cycles were obtained, but this could be overcome by changing the default step size, except HCNOLi(II); therefore, in the case of HCNOLi(II), harmonic frequencies were calculated using the B3LYP/6-311++G** method. Dipole moments and total atomic charges were calculated using the QCISD density and the natural population analysis. All calculations were performed with the Gaussian-94 quantum chemistry package[32] implemented on Silicon Graphics, Inc. Challenge/XL and Origin200 workstations.

The ionization potentials for NNO, HCNO, and HNNN were calculated using the outer valence Green's function (OVGF) method[33] as incorporated in Gaussian-94, and also with the semiempirical HAM/3 (hydrogenic atoms in molecules) method,[34] which was shown to give an accurate representation of IPs for molecules containing first-row atoms.[35] OVGF and HAM/3 calculations were performed at the experimental geometries of molecules.[30]

IV. Results

Figures 1−3 show the He I UPS and He*(2^3S) PIES spectra of NNO, HCNO, and HNNN, respectively. The electron energy scales for PIES spectra are shifted relative to those of UPS by the difference in the excitation energies; 21.22−19.82 = 1.40 eV.

Figures 4−6 show the CERPIES spectra of NNO, HCNO, and HNNN, respectively. The spectra are obtained from the 2D-PIES spectra by cutting a small kinetic energy region corresponding to ca. 20 μs TOF of He*. In each figure, the low collision energy spectrum (ca. 90−110 meV, average 100 meV) is shown by a dashed curve, and the high collision energy spectrum (ca. 220−290 meV, average 250 meV) is shown by a solid curve.

Figures 7−9 show the log σ vs log E_c plots of CEDPICS for NNO, HCNO, and HNNN, respectively. The CEDPICS are obtained from the 2D-PIES spectra by cutting an appropriate range of electron kinetic energy, E_e (typically the fwhm of the corresponding PIES band). The calculated electron density maps of the molecular orbitals are also shown in the figures (the thick solid curve in maps indicates the molecular surface, estimated from the van der Waals radii of atoms); electron density contour maps in a symmetry plane of the molecule are shown for the orbitals of NNO and HCNO, as well as for the a′ orbitals of HNNN. For the a″ orbitals of HNNN, one of those planes is selected, which are parallel to the symmetry plane of the molecule and lying just above the van der Waals radius of nitrogen.

Figures 10−12 show calculated potential energy curves between a ground-state Li atom and NNO, HCNO, and HNNN,

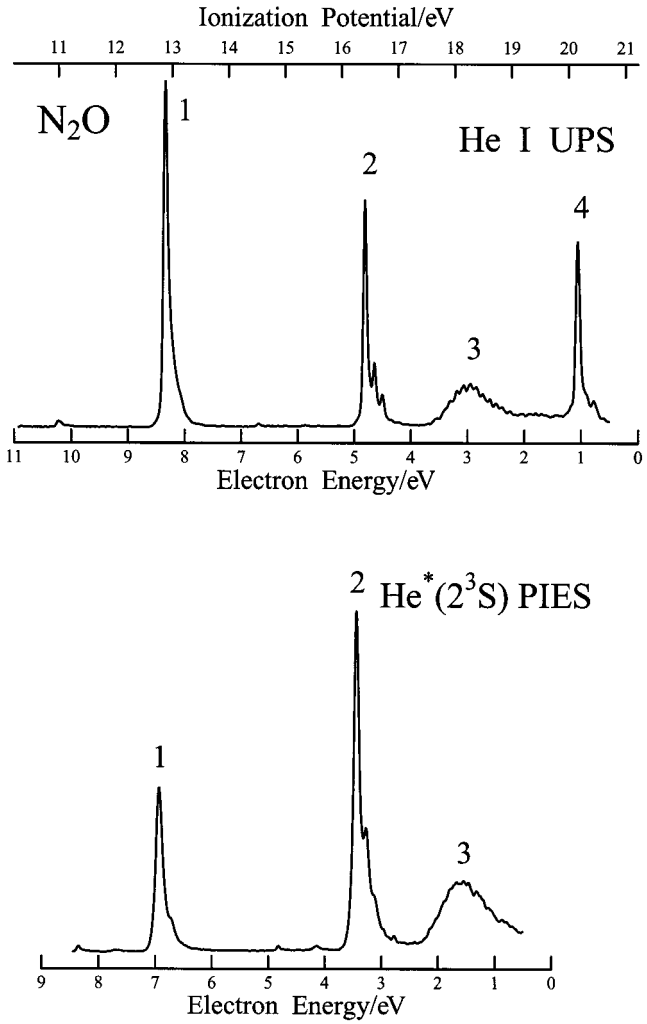

Figure 1. He I UPS and He*(2³S) PIES spectrum of NNO.

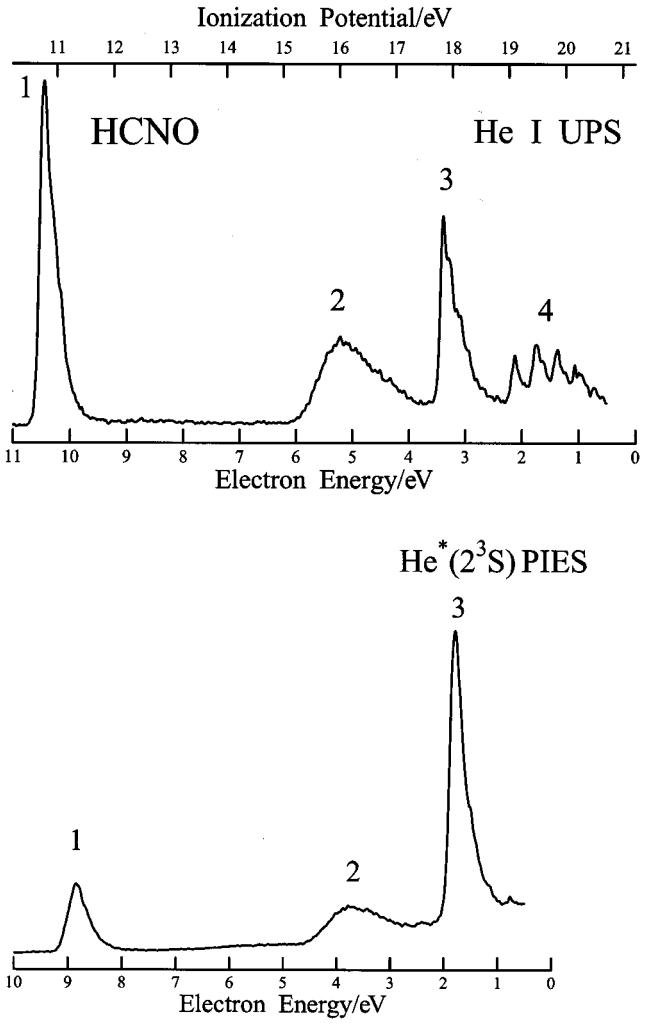

Figure 2. He I UPS and He*(2³S) PIES spectrum of HCNO.

respectively. The potential energy is shown as a function of the distance between the Li atom and the center of mass of the molecule. Calculations are done at the CCSD(fc)/6-311++G** level of theory.

Figure 13 shows the calculated structure of HCNOLi and HNNNLi radicals, as well as the calculated total atomic charges (natural population analysis was done using the QCISD density). Calculations were done at the QCISD(fc)/6-311++G** level of theory.

Figure 14 illustrates the major orbital interactions between HNNN and Li, explaining the formation of HOMO and LUMO of HNNNLi. Orbital energies were calculated at the QCISD-(fc)/6-311++G** geometries.

Figure 15 shows the major orbital interactions between HCNO and Li, explaining the formation of the HOMOs and LUMOs of HCNOLi(I and II) isomers. Orbital energies were calculated at the QCISD(fc)/6-311++G** geometries.

Table 1 lists experimental and calculated ionization potentials (IPs), experimental peak energy shifts (ΔE), slope parameters (m), and the assignment of the spectra. Slope parameters are obtained from the log σ vs log E_c plots (for details of explaining the expected linear relationship between log σ and log E_c see, e.g., ref 1). Vertical IPs are determined from the He I UPS spectra. The peak energy shifts in PIES spectra are obtained as the difference between the peak position (E_{PIES}; electron energy scale) and the "nominal" value (E_0 = difference between the metastable excitation energy and target IP), $\Delta E = E_{PIES} - E_0$.

Table 2 lists calculated harmonic vibrational frequencies, infrared intensities, rotational constants, dipole moments, total energies, barriers to linearity or planarity, and bonding energies of HCNOLi and HNNNLi radicals. Calculated results at the QCISD(fc)/6-311++G** level of theory are shown, except the harmonic vibrational frequencies and IR intensities of HCNOLi-(II), which were obtained at the B3LYP/6-311++G** level.

V. Discussion

A. UPS and PIES Spectra. Since the information derived on the interaction potential in the sequence of removing an electron from a MO → formation of ionic state → collision energy dependence of the ionization cross section → interaction potential strongly depends on the localization of MOs, it is important to unambiguously assign the UPS/PIES bands. From comparison with the known UPS spectra of NNO[17,18] and HCNO,[19] as well as from the calculated IPs (see Table 1), the assignment for NNO and HCNO is relatively straightforward, especially since, for these linear molecules, there is a complete π/σ separation. Our assignment (Table 1) confirms previous investigations. Four bands are observed in the He I UPS spectrum of NNO, which originate, in the order of increasing IPs, from the degenerate nonbonding π_{nb}(NNO), nitrogen lone pair n_N, and degenerate bonding π_b(NNO) orbitals, as well as the oxygen lone pair orbital n_O. In the case of HCNO, the four observed UPS bands originate from the degenerate nonbonding π_{nb}(CNO) and bonding π_b(CNO) orbitals, as well as the oxygen

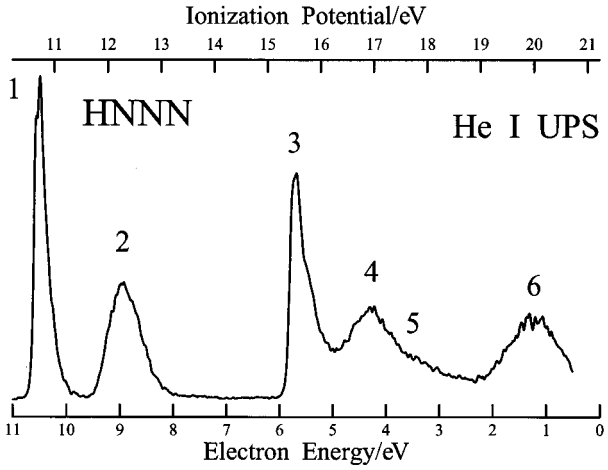

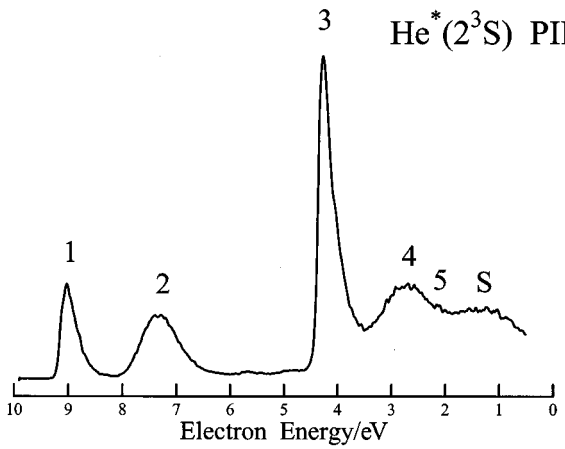

Figure 3. He I UPS and He*(2^3S) PIES spectrum of HNNN.

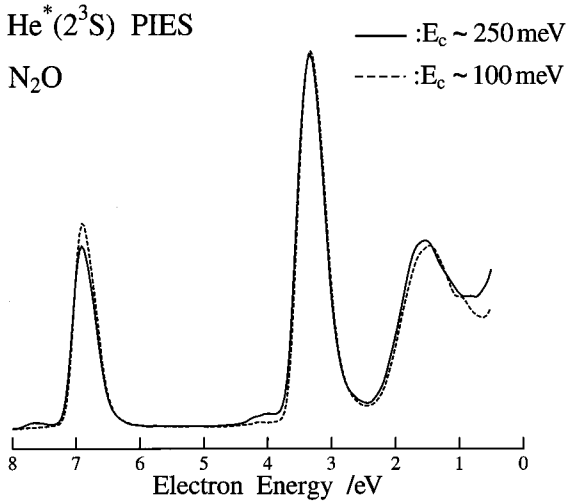

Figure 4. Collision energy resolved He*(2^3S) PIES spectra of NNO.

lone pair orbital n_O, and σ(C−H) orbital. Due to the slightly smaller excitation energy of He*(2^3S) than He I photons, the fourth bands at higher IPs are not observed in PIES spectra. On the basis of three bands in the PIES spectra of NNO and HCNO, therefore, information on the interaction potential can be deduced around the π region and at one end of the linear frame at the nitrogen and oxygen lone pair, respectively. The π_b orbitals have higher electron density at the central nitrogen atom, but π_{nb} has a nodal surface here and more localized on

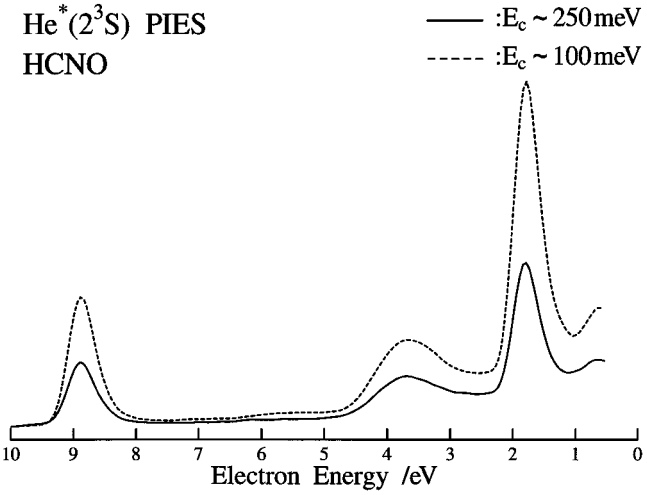

Figure 5. Collision energy resolved He*(2^3S) PIES spectra of HCNO.

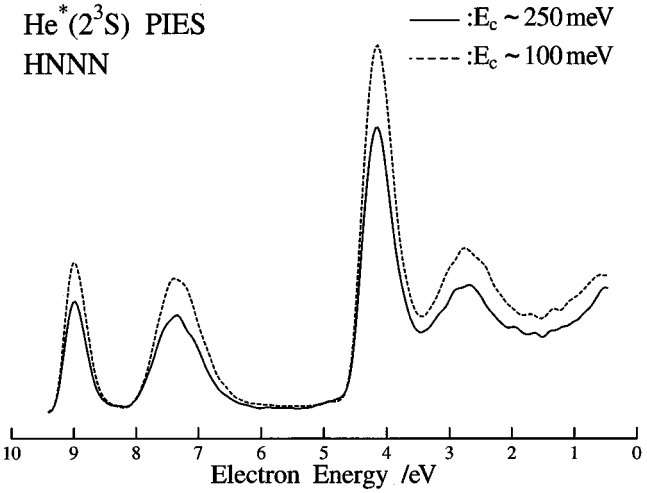

Figure 6. Collision energy resolved He*(2^3S) PIES spectra of HNNN.

the end atoms of the NNO or CNO group; thus, the two π orbitals probe different parts of the interaction potential surface (see Figures 7 and 8).

HNNN is not a linear molecule. If it were linear, the MOs of HNNN would be of the same character as those of NNO and HCNO, and the π orbitals would remain degenerate. In the real molecule, however, the degeneracy of both the bonding and nonbonding π orbitals is lifted to produce two pairs of orbitals of symmetry a″ and a′. In the simplest model (see Scheme 2) the orbital a′ derived from the nonbonding π orbital becomes a lone pair on the nitrogen atom and the a′ orbital derived from the bonding π orbital becomes a pure N═N bond. The out-of-plane orbitals retain their original π character. The extent of the lone pair and double bond character, or their delocalization, however, depends on the deviation from linearity, and in the practical case, both the delocalized and localized model (2a and 2b in Scheme 2) can serve as a starting point of the description of the electronic structure of HNNN and can be regarded as the two most important mesomeric structure. For the simplest discussion, we use the π_{nb} and π_b symbols for HNNN as well, similar to NNO and HCNO, but we have to keep in mind the structural difference suggested by the model 2b in Scheme 2. Six bands are observed in the He I UPS spectrum of HNNN, the fifth is only as a weak shoulder at 17.7 eV (Figure 3). This band was not observed, due to a purer signal/noise ratio in previous He I investigations,[19−21] but is detected in the most recent He II work of Lee et al.[21] Probably the lack of observing

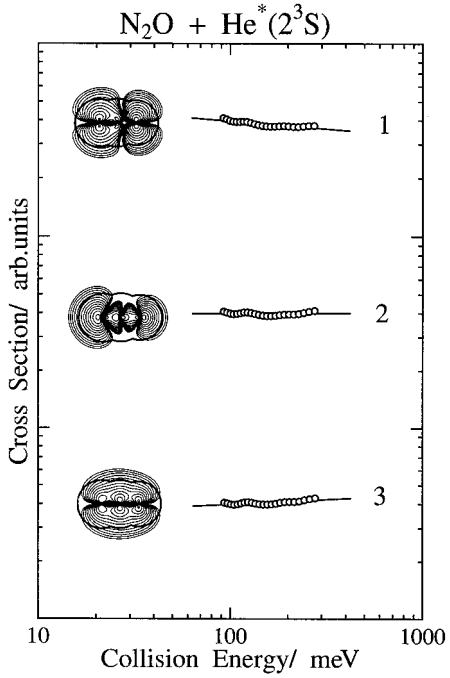

Figure 7. Collision energy dependence of partial ionization cross sections for NNO with He*(2^3S).

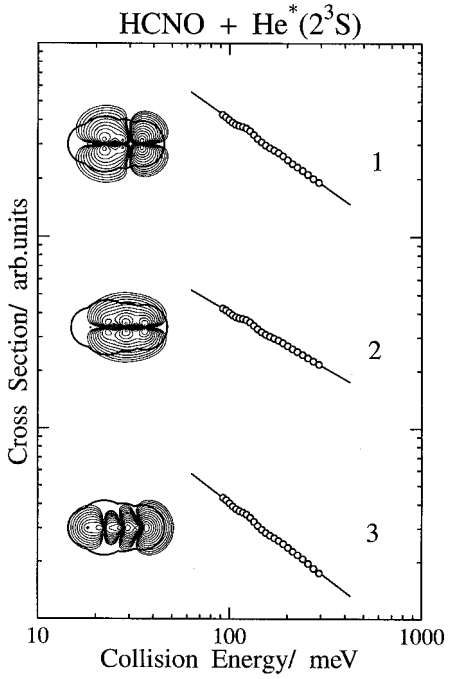

Figure 8. Collision energy dependence of partial ionization cross sections for HCNO with He*(2^3S).

this band, as well as the failure of Koopmans theorem to predict reliable IPs for pseudohalides in the high IP region, is the reason that in previous works the high IP region is misassigned suggesting an exceptionally large splitting of 2.7−3.8 eV between π_b(a″) and π_b(a′).[19,20c,21] Our new assignment (see Table 1) is based on our new calculations, in agreement with a previous calculation using Rayleigh−Schrödinger perturbation theory to determine corrections to Koopmans' theorem,[36] and careful comparison between the UPS spectra of isovalence electronic molecules HNNN, HNCO, and HNCS.[20a,37] These all suggest that the splitting between π_b(a″) and π_b(a′) must be smaller than 1 eV. This is also in good agreement with the

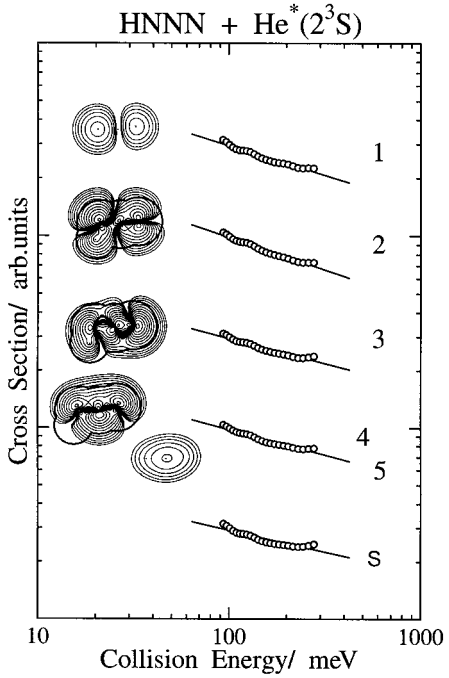

Figure 9. Collision energy dependence of partial ionization cross sections for HNNN with He*(2^3S).

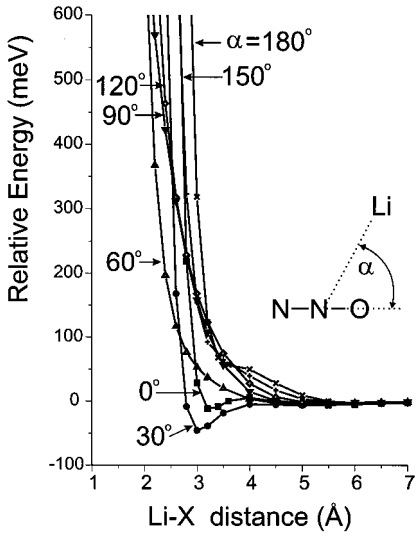

Figure 10. Calculated interaction potential curves between NNO and Li(2^2S) as functions of distance between the Li atom and the center of mass of the molecule.

previous comment of Eland that the splitting between in-plane and out-of-plane π orbitals of pseudohalo acids is less for the bonding than for the nonbonding ones.[20a] The six bands in the He I UPS spectrum of HNNN thus originate, in the order of increasing IPs, from the nonbonding π_{nb}(a″) and π_{nb}(a′), nitrogen terminal lone pair n_N, and π_b(a″) and π_b(a′) orbitals, as well as the σ(N−H) orbital. This latter one is not observed in the PIES spectrum due to the He*(2^3S) cut off. There is, however, an additional peak in the PIES spectrum in the high IP region (marked with "S" in Figure 3), which is not observed in He I UPS, and we believe it arises from simultaneous ionization−excitation "shake-up" process. Penning spectroscopy is known to enhance two-electron processes, and it is also known that their probability increases by increasing the photon energy in photoelectron spectroscopy. Indeed, a small feature can be seen in the He II UPS (Figure 2 in ref 21) at the same place between

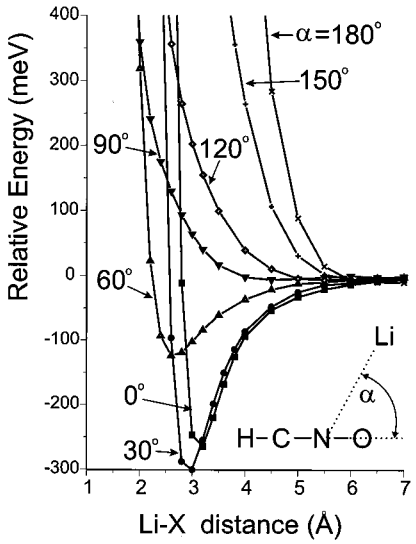

Figure 11. Calculated interaction potential curves between HCNO and Li(2^2S) as functions of distance between the Li atom and the center of mass of the molecule.

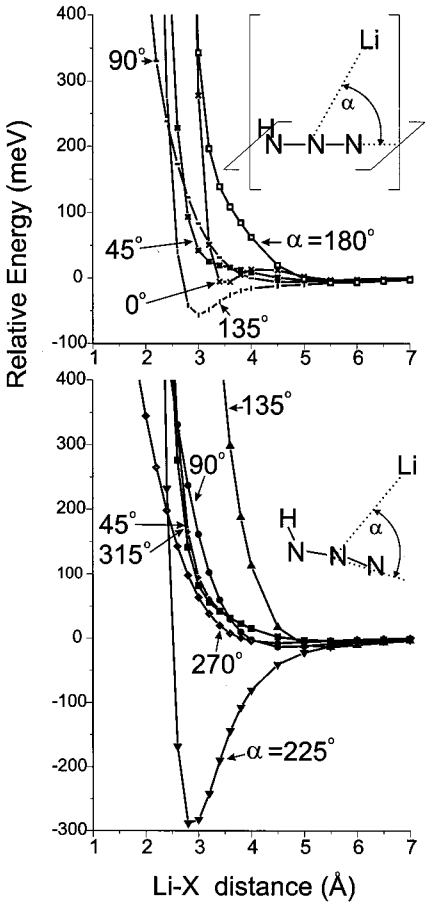

Figure 12. Calculated interaction potential curves between HNNN and Li(2^2S) as functions of distance between the Li atom and the center of mass of the molecule.

18 and 19 eV. According to the observed PIES bands, therefore, the interaction potential can be investigated in the π region and the nitrogen terminal lone pair region of HNNN.

The PIES spectra of NNO, HCNO, and HNNN are shown in Figures 1−3. The branching ratios are clearly different compared to those in UPS spectra, which reflect the difference in the ionization mechanism; strong bands in PIES originate from

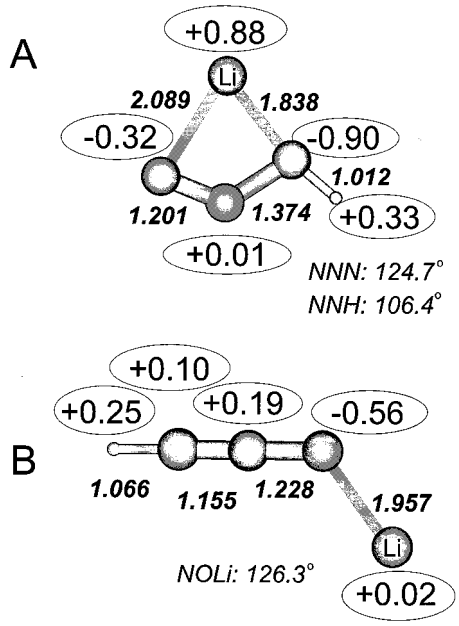

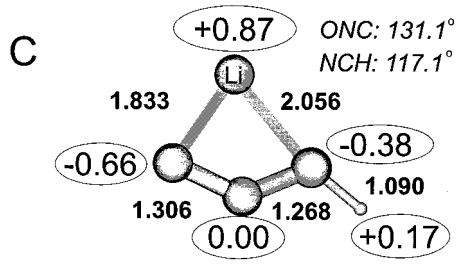

Figure 13. Calculated structure (distances in angstrom) and total atomic charges of HNNNLi (A), HCNOLi(I) (B), and HCNOLi(II) (C) radicals.

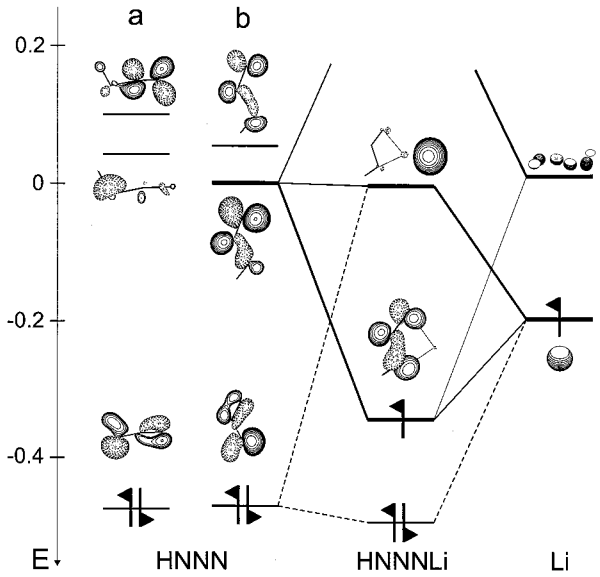

Figure 14. Major orbital interactions between HNNN and Li explaining the formation of HOMO and LUMO of HNNNLi (energy scale is given in atomic units). Orbitals with a″ symmetry are not shown in the figure for clarity. Orbitals of HNNN are shown at the equilibrium geometry (a) and at the geometry in the complex (b).

orbitals having large electron density exposed outside to the molecular surface. A general feature of the PIES spectra of the investigated molecules is that the terminal lone pair band (n_N or n_O) is strongly enhanced, especially in case of HCNO (note

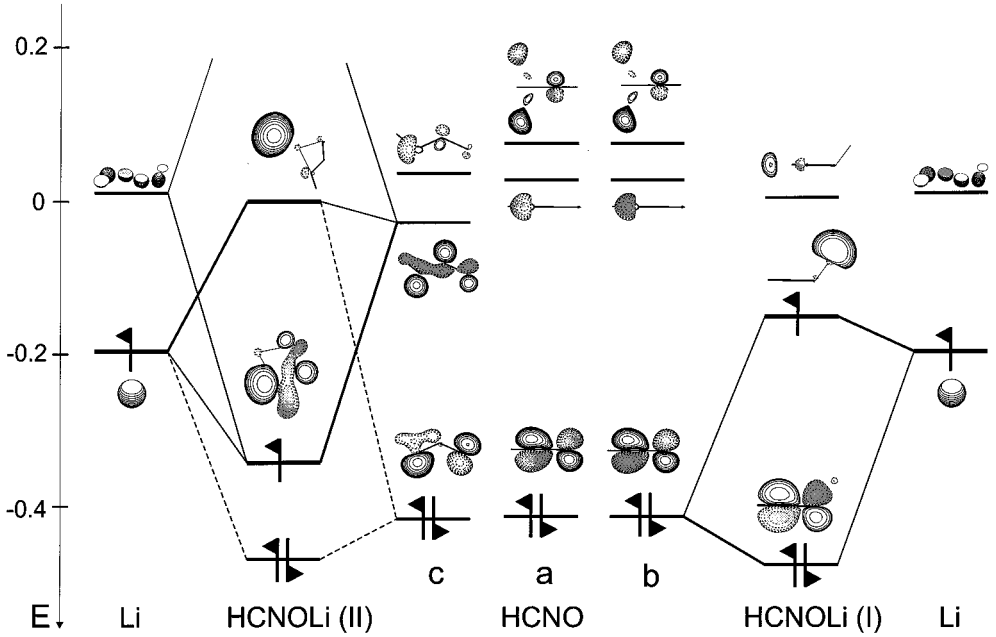

Figure 15. Major orbital interactions between HCNO and Li explaining the formation of the HOMOs and LUMOs of HCNOLi(I) and HCNOLi-(II) (energy scale is given in atomic units). Orbitals with a″ symmetry are not shown in the figure for clarity. Orbitals of HCNO are shown at the equilibrium geometry (a) and at the geometry in the complex (b, c).

TABLE 1: Band Assignments, Ionization Potentials (IP/eV), Peak Energy Shifts (Δ*E*/meV), and Slope Parameters (*m*) for NNO, HCNO, and HNNN

		IP/eV			orbital	Δ*E*/meV	*m*
molecule	band	exptl	HAM3	OVGF	character	(±20 meV)	(±0.03)
NNO	1	12.88	12.48	12.56	$2\pi(\pi_{nb})$	−15	−0.08
	2	16.41	16.51	16.55	$7\sigma(n_N)$	+20	0.00
	3	18.07	18.67	18.87	$1\pi(\pi_b)$	+20	+0.05
	4	20.16	20.68	20.64	$6\sigma(n_O)$		
HCNO	1	10.77	10.92	10.61	$2\pi(\pi_{nb})$	−200	−0.70
	2	16.00	17.07	16.77	$1\pi(\pi_b)$	−65	−0.58
	3	17.84	18.77	18.38	$7\sigma(n_O)$	−210	−0.78
	4	19.47	20.70	20.11	6σ(CH)		
HNNN	1	10.73	10.38	10.24	$2a''(\pi_{nb})$	−70	−0.31
	2	12.28	12.05	12.02	$9a'(\pi_{nb})$	−205	−0.34
	3	15.53	15.36	15.96	$8a'(n_N)$	−40	−0.26
	4	16.92	17.31	17.07	$1a''(\pi_b)$	−215	−0.27
	5	(17.7)	17.27	17.21	$7a'(\pi_b)$		
	6	19.91	20.47	20.74	$6a'(\sigma$NH)		

that π bands are doubly degenerate). Similar enhancements were observed recently in spectra of nitriles,[1,16] isocyanates, and isothiocyanates;[13] thus, this seems to be a characteristics of the pseudohalide group and may explain the good complexing ability of pseudohalides via terminal lone pair dative bond. Peak shifts in PIES spectra are clearly observed. These are small, around zero, for NNO in good agreement with previous investigations[22,23] and predict that there is no strong interaction between NNO and He*(2^3S), and large collision energy dependence of the ionization cross section is not expected. This is in good agreement with the observed very small collision energy dependence of the PIES branching ratios and partial cross sections for the production of different ions in a previous PIES and mass spectroscopic study, respectively, at two different beam temperatures.[23] Although the total ionization cross section is not expected to depend on the collision energy, the small peak shifts indicate that the interaction potential is not isotropic around the molecule; the peak shift is slightly negative (−15 meV; Table 1) for the first band and positive (+20 meV) for the second and third, which, regarding the localization of MOs, indicates a small attractive interaction around the oxygen atom. The peak shifts in PIES spectra of HCNO and HNNN are negative for all bands, and in some cases, they are large negative values of ca. −200 meV (see Table 1), which indicate that the interaction between these molecules and He*(2^3S) is very attractive. The peak shifts also show that the interaction potential is anisotropic around the molecules. In the case of HCNO, there is a large negative peak shift for the oxygen lone pair band and for π_{nb}(CNO) band. The π_{nb}(CNO) orbital also has a large electron density on the oxygen atom; thus, according to the peak shifts, the most attractive part of the attractive surface must be around the oxygen atom. The splitting between π_{nb}(a″) and π_{nb}(a′) peaks in PIES spectrum of HNNN is large enough to observe peak shifts separately. There is a large negative peak shift for the π_{nb}(a′) band, which indicates that the interaction potential is attractive in the π_{nb}(a′) orbital region. This MO has imine-type nitrogen lone pair character (see Scheme 2), and probably this lone pair region is the most attractive part of the molecule. Since the π_b(a′) orbital also has large electron density in the same region, the large negative peak shift for this latter is in agreement. The peak shift is much smaller for the π_{nb}(a″) band, which shows that the interaction is less attractive if the metastable atom approaches the molecule perpendicular to the molecular plane compared to the in plane direction. The peak shift of −40 meV for the terminal nitrogen lone pair n_N band is surprisingly small, although it shows attractive interaction, compared to that of the nitrogen lone pair of alkyl nitriles, where a large peak shift (−270 to −390 meV) and very attractive potential has been observed.[1,16] Probably the three electronegative nitrogen atoms, and thus the smaller electron density on the terminal nitrogen, are responsible for the less attractive interaction. Regarding the attractivity of the terminal nitrogen lone pair region, HNNN is between the nitrogen molecule N_2, where the interaction is repulsive,[38] and R−CN, where it is very attractive.

B. 2D PIES and Interaction Potential. One-dimensional cuts of 2D-PIES spectra, CERPIES and CEDPICS spectra are shown in Figures 4−6 and 7−9, respectively, and calculated Li−M interaction potential curves are shown in Figures 10−12. The 2D-PIES investigation on NNO indicates that there is practically no collision energy dependence of the total ionization cross

TABLE 2: Calculated Vibrational Frequencies (cm^{-1}), IR Intensities (km/mol), Rotational Constants (GHz), Dipole Moments (Debye), Total Energies (au), Barrier (cm^{-1}), and Bonding Energy (kJ/mol) of HCNOLi and HNNNLi[a]

HCNOLi(I)		HCNOLi(II)		HNNNLi	
frequency	IR int	frequency[b]	IR int[b]	frequency	IR int
3499 ν_1(C−H str)	305.0	3137 ν_1(C−H str)	1.0	3623 ν_1(N−H str)	9.7
2330 ν_2(CNO as str)	178.0	1593 ν_2(CN str)	197.6	1688 ν_2(N≡N str)	128.5
1212 ν_3(CNO sym str)	165.4	1163 ν_3(NO str)	25.4	1363 ν_3(H−NN in-plane def)	98.3
530 ν_4(CNO in-plane bend)	10.0	974 ν_4(H−CN in-plane def)	276.2	935 ν_4(N═N str)	213.0
510 ν_8(CNO out-of-plane bend)	8.1	679 ν_8(H−CN out-of-plane def)	49.3	694 ν_5(ring in-plane vib)	21.8
399 ν_5(H−CN in-plane def)	51.7	671 ν_5(ring in-plane vib)	35.3	613 ν_6(H−NN out-of-plane def)	70.5
364 ν_6(Li−O str)	9.4	565 ν_6(ring in-plane vib)	107.6	542 ν_7(ring in-plane vib)	64.5
354 ν_9(H−CN out-of-plane def)	43.6	425 ν_7(ring in-plane def)	16.0	319 ν_8(ring in-plane def)	55.0
112 ν_7(Li−ON def)	50.1	223 ν_9(ring out-of-plane def)	71.7	102 ν_9(ring out-of-plane def)	99.3

HCNOLi(I)		HCNOLi(II)		HNNNLi	
A[c]	63.8374	A[c]	24.6405	A[c]	22.0870
B	6.0183	B	11.7338	B	12.4914
C	5.4998	C	7.9487	C	7.9992
μ[d]	7.28 (8.53)	μ[d]	4.33 (4.15)	μ[d]	4.56 (4.80)
total energy	−175.644992	total energy	−175.687386	total energy	−171.901701
bonding energy[e]	37.7	bonding energy[e]	149.0	bonding energy[e]	143.9
barrier[f]	590.6			barrier[g]	0.8

[a] Calculated at the QCISD/6-311++G** level of theory. [b] Calculated at the B3LYP/6-311++G** level of theory. [c] Isotopes: H-1, C-12, N-14, O-16, Li-7. [d] Population analysis was done using the QCISD (SCF) density. [e] Difference between the total energy of the complex and the sum of the energies of fragments. [f] Barrier to linearity. [g] Barrier to planarity.

SCHEME 2

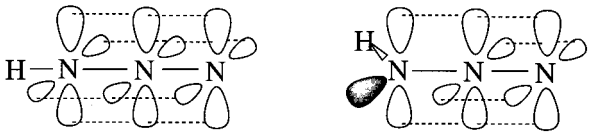

2a 2b

section (slope parameter $+0.01 \pm 0.03$), and the dependence of the partial ionization cross sections is very small, close to zero (see Table 1). This latter, however, indicates small anisotropy of the interaction potential, which is in good agreement with the calculated Li−NNO potentials. According to the calculations, the most attractive part of the molecule is the oxygen lone pair region (the IP of the corresponding orbital n_O is beyond the He*(2^3S) cut off, thus, not investigated experimentally), not the collinear direction though, but around the Li−N−O angle of 30°, and the attractive potential gradually changes to repulsive as the Li−N−O angle opens up to 180°. Since π_{nb}(NNO) MO has large electron density on the oxygen atom, and π_b(NNO) MO has the largest on the central nitrogen atom, the small negative collision energy dependence of the intensity of the π_{nb}(NNO) band and small positive of the π_b(NNO) band is in good agreement with calculations. The n_N MO is partially mixed with n_O (see Figure 7) and thus probes to some extent the oxygen lone pair region as well, which explains the smaller positive collision energy dependence of the n_N band than that of π_b(NNO). The interaction between HCNO and He*(2^3S) is very attractive in the π and n_O region (see Figures 5 and 8). According to our experience, it is very rare to observe such a large negative collision energy dependence of the ionization cross section between molecules and He*(2^3S) atoms (see Table 1). The largest negative dependence is observed at the n_O band and then at the π_{nb}(CNO), which indicates that the most attractive part of the molecule is around the oxygen atom. This is in good agreement with calculations (Figure 11), showing a very attractive potential with deep well, when the lithium atom approaches the molecule at the oxygen, and this attractive potential gradually changes to repulsive as the Li−N−O angle opens up. According to the calculations, the interaction is repulsive around the hydrogen atom. The 2D-PIES experiment shows that the interaction is attractive between HNNN and He*(2^3S) around the NNN group (Figures 6 and 9). There are no large differences between the collision energy dependence of the partial ionization cross sections (see slope parameters in Table 1), but the largest negative dependence is observed at the π_{nb}(a′) band. In good agreement with the observed peak shifts, this indicates that the region of the corresponding π_{nb}(a′) orbital, which has imine type lone pair character, is the most attractive part of the molecule. Indeed, the calculated Li−M potentials clearly indicate this "lone pair" region as the most attractive part (Figure 12), and the attractivity of the interaction is decreased as Li atom approaches at the other end of the NNN group. Similarly to HCNO, the interaction is repulsive around the hydrogen atom.

In general, there is a very good agreement between experimental peak shifts, collision energy dependence of the partial ionization cross sections, and calculated Li−M interaction potentials. These show that the interaction potential is attractive around the π and the terminal oxygen or nitrogen lone pair region of −CNO and −NNN groups. The isoelectronic NNO molecule has a similar electronic structure, especially compared to HCNO, but the interaction is not attractive with He*(2^3S) or Li(2^2S). When the oxygen or nitrogen atom in this molecule is replaced by a HN or CH fragment, however, the −NNN and −CNO groups acquire a negative charge,[39] which may responsible for the attractive interaction. Indeed, the most attractive part of each molecule is on the most negatively charged atom, and the positive hydrogen represents an opposite, repulsive character. The total atomic charges, however, do not explain the anisotropy of the electron density around atoms or chemical groups, this can be obtained from the analysis of the molecular orbital picture (see above). In this respect, the collision energy dependence of the partial ionization cross sections, depending on the localization of MOs, indicates the large electron density regions of the molecules.

C. HNNNLi and HCNOLi Radicals. The negative collision energy dependence of the ionization cross section and the large negative peak shift of the corresponding PIES band indicate that there is a deep well on the interaction potential curve, which indirectly predicts the existence of thermodynamically stable MLi radicals. This is also in good agreement with the M−Li

model potential calculations. According to these results (see above), two complexes are expected to be thermodynamically the most stable: one is the HCNOLi, where the Li is expected to bond to the oxygen atom, and the second is HNNNLi, where Li is attached to the imine type nitrogen lone pair ($\pi_{nb}(a')$). It is important to note, however, that due to the fast speed of metastable atoms and instantaneous ionization compared to the molecular nuclear motion, the geometry of the molecules is nearly frozen in the Penning ionization process, which is not the case in a chemical reaction between molecules and Li atoms. Due to geometry relaxation, the bonding energy of MLi complexes can be much larger than is predicted from the peak energy shifts in PIES (depth of the interaction potential). This relaxation is strongly depend on the reacting systems and cannot be predicted in advance. To get information about the stability and also the structure of these radicals, ab initio calculations have been performed for the structure of HCNOLi and HNNNLi. Calculated results are shown in Figure 13 and Table 2. Full geometry optimizations at the QCISD level ran into the expected minima of HNNNLi and HCNOLi(I) (I denotes isomer I, see below). The structure of HCNOLi(I) may be best characterized as a classical complex, where the HCNO ligand bonds at the oxygen atom to Li with a coordinative bond. The total atomic charge on Li is close to zero (+0.02), and the lithium unpaired electron stays on Li. The geometry of HCNO does not change significantly, and the molecule keeps its close linear structure in the complex. The bond angle at the oxygen is 126.3°, and the barrier of HCNOLi(I) to linearity is 590.6 cm^{-1}, which is fairly low but definitely higher than the low lying vibrational levels (the calculated harmonic frequency of the N−O−Li bend is 112 cm^{-1}). The structure and bonding of HNNNLi is very different compared to that of HCNOLi(I). HNNNLi is a π-type complex, where the Li atom bonds to both ends of the NNN group forming a four-membered ring. The equilibrium structure of the complex is not planar, but the barrier to planarity is a mere 0.8 cm^{-1}; thus, all vibrational levels lie above this and the molecule has a quasiplanar structure. The unpaired electron of the Li atom completely delocalizes on the HNNN σ frame, and as a consequence there is a positive charge of +0.88 on the Li atom. There is a large difference in the bonding energies of these two complexes (37.7 and 143.9 kJ/mol; Table 2). To understand the difference in bonding, the formation of MOs of complexes from orbitals of their fragments have been investigated, and results explaining the formation of HOMOs are shown in Figures 14 and 15. As Figure 14 illustrates, the LUMO of HNNN is strongly stabilized by the interaction of HNNN and Li, and the transfer of the lithium 2s electron into this lower lying empty orbital explains the large bonding energy of the complex. In the case of HCNOLi(I), the LUMO(HCNO)−LUMO(Li) interaction is small and the formation of HOMO is mainly HOMO(HCNO)−HOMO(Li) controlled. The HOMO of HCNO is stabilized, and the HOMO of Li is destabilized; thus, there is a smaller energy benefit of this process than is the case for HNNNLi. It seems that the formation of a lower lying LUMO due to the bending of the NNN frame, which can strongly interact with one of the 2p orbitals of Li, is responsible for the large stabilization energy of the HNNNLi complex. The difference between HCNO and HNNN in the complex formation was surprising first, especially since model calculations indicated the same change in electronic stucture as that of HNNN by bending the CNO frame, but a search for possible HCNOLi isomers identified the four-membered ring π-complex HCNOLi(II). The structure and bonding of this complex are very similar to those of HNNNLi (Figure 13 and Table 2): the unpaired electron is delocalized on the CNO frame, the charge on Li atom is +0.87, and the bonding energy is large (149.0 kJ/mol). This complex is thermodynamically much more stable than HCNOLi(I). During the QCISD potential energy surface scan, divergence in the post-HF iteration cycles has been experienced many times, as well as in the frequency calculations; therefore, the structure of HCNOLi(II) was recalculated at the B3LYP level (see ref 40), which is in good agreement with the QCISD results and confirms HCNOLi(II) as a planar four-membered ring. From the model potential calculations, it is clear that HNNNLi and HCNOLi(I) can form from Li and HNNN and HCNO, respectively, without any kinetic barrier. To obtain information on the formation of HCNOLi(II) and the kinetic stability of HCNOLi(I), a potential surface scan was done at the B3LYP level (due to divergence problems in QCISD again). According to B3LYP calculations, HCNOLi(II) forms from Li and HCNO without any kinetic barrier and HCNOLi(I) is only a local minimum on the way to the formation of HCNOLi(II) (the barrier of the isomerization of HCNOLi(I) into HCNOLi(II) is 5.6 kJ/mol; see ref 41). Calculations, therefore, predict that, in both HCNOLi and HNNNLi, the π-complex is the only stable form. The identification of both HCNOLi and HNNNLi is feasible either in an inert solid matrix or in the dilute gas phase. To support future identifications, calculated harmonic frequencies, infrared intensities, rotational constants, and dipole moments are shown in Table 2. Recently, there has been much interest in cluster chemistry to study the development of solvation from small complexes to the bulk phase, and one of the most interesting questions in alkali atom interaction with polar solvent is the delocalization of the atomic valence electron as more and more polar molecules are bonded to the atom.[42] In this respect, the alkali metal HNNN and HCNO interactions may present interesting challenges as the valence electron delocalization can possibly be achieved with very small cluster sizes.

VI. Conclusion

The isoelectronic molecules NNO, HCNO, and HNNN have been investigated in the gas phase through a combination of electron spectroscopic and ab initio methods. Experiments show that the interaction potentials between He*(2^3S) metastable atoms and molecules are anisotropic and the interactions of He*(2^3S) with NNO, HCNO, and HNNN are very different compared to each other, reflecting the difference in the electronic structures. The interaction between HCNO and He*(2^3S) is unusually attractive, especially around the oxygen atom. Attractive interaction has been found between HNNN and He*(2^3S), too, having the most attractive part at the imine type nitrogen lone electron pair region. The interaction between He*(2^3S) and NNO is not characteristic, not attractive nor repulsive; the total ionization cross section does not show any collision energy dependence, but the small dependencies of partial ionization cross sections indicate that the interaction is slightly attractive around the oxygen atom and slightly repulsive at the other end of the molecule. A common feature of the electronic structure of the investigated molecules is that the electron density of terminal lone pair orbitals is exposed strongly outside the molecular surface, indicating places for electrophile attack. Our investigation on HNNN, however, also shows that this large electron density outside the molecular surface does not necessarily indicate the largest electron density part of the molecule, which strongly determines the most attractive side of the molecule. Ab initio calculations reveal fine details of the Li−M(molecule) interaction potentials and are in good agree-

ment with the experimental results. They, furthermore, provide information about the H atom region of the molecules, which could not be probed by experiment, and indicate that the interaction potential is repulsive around the hydrogen atom.

Both experimental and calculated results indicate the existence of stable Li−M radicals, among those the thermodynamically most stables are the four-membered rings HCNOLi and HNNNLi. According to QCISD calculations, the unpaired electron of the lithium atom completely delocalizes on the CNO or NNN frame, and the stabilization of this latter explains the large bonding energy of these π-type complexes. The formation of π-complex and delocalization of the lithium valence electron is an interesting result of this work, and we plan to further investigate this. Our preliminary calculations on similar systems, such as HNCO + Li, HNCS + Li, and NCCN + Li, indicate the same effect found in this work, namely, the π-complex formation results in the delocalization of the metal unpaired electron and large bonding energy.

Acknowledgment. We thank the Japanese Ministry of Education, Science, and Culture for a Grant in Aid for Scientific Research in support of this work. T.P. thanks the Japan Society for the Promotion of Science (JSPS) for a JSPS Invitation Fellowship (IDNo. L98519) and the Hungarian Scientific Research Found (OTKA Grant F022031) in support of this work.

References and Notes

(1) Pasinszki, T.; Yamakado, H.; Ohno, K. *J. Phys. Chem.* **1995**, *99*, 14678.

(2) Ohshimo, K.; Tsunoyama, H.; Yamakita, Y.; Misaizu, F.; Ohno, K. *Chem. Phys. Lett.* **1999**, *301*, 356.

(3) Kasai, P. H. *J. Am. Chem. Soc.* **1998**, *120*, 7884.

(4) Ohno, K.; Yamakado, H.; Ogawa, T.; Yamata, T. *J. Chem. Phys.* **1996**, *105*, 7536.

(5) (a) Kishimoto, N.; Yamakado, H.; Yamata, T.; Ogawa, T.; Ohno, K. *Int. Conf. Phys. Electron. At. Collisions*, 19th, **1995**, *1995*, 807. (b) Auerbach, D. J. In *Atomic and Molecular Beam Methods*; Scoles, G., Ed.; Oxford University Press: New York 1988; p 369.

(6) Takami, T.; Mitsuke, K.; Ohno, K. *J. Chem. Phys.* **1991**, *95*, 918.

(7) Takami, T.; Ohno, K. *J. Chem. Phys.* **1992**, *96*, 6523.

(8) Ohno, K.; Okamura, K.; Yamakado, H.; Hoshino, S.; Takami, T.; Yamauchi, M. *J. Phys. Chem.* **1995**, *99*, 14247.

(9) Yamakado, H.; Yamauchi, M.; Hoshino, S.; Ohno, K. *J. Phys. Chem.* **1995**, *99*, 17093.

(10) Kishimoto, N.; Yamakado, H.; Ohno, K. *J. Phys. Chem.* **1996**, *100*, 8204.

(11) Yamauchi, M.; Yamakado, H.; Ohno, K. *J. Phys. Chem. A* **1997**, *101*, 6184.

(12) Yamakado, H.; Ogawa, T.; Ohno, K. *J. Phys. Chem. A* **1997**, *101*, 3887.

(13) Pasinszki, T.; Yamakado, H.; Ohno, K. *J. Phys. Chem.* **1993**, *97*, 12718.

(14) Ohno, K.; Kishimoto, N.; Yamakado, H. *J. Phys. Chem.* **1995**, *99*, 9687.

(15) Kishimoto, N.; Yokoi, R.; Yamakado, H.; Ohno, K. *J. Phys. Chem. A* **1997**, *101*, 3284.

(16) Kishimoto, N.; Aizawa, J.; Yamakado, H.; Ohno, K. *J. Phys. Chem. A* **1997**, *101*, 5038.

(17) (a) Brundle, C. R.; Turner, D. W. *Int. J. Mass Spectrom. Ion Phys.* **1969**, *2*, 195. (b) Dehmer, P. M.; Dehmer, J. L.; Chupka, W. A. *J. Chem. Phys.* **1980**, *73*, 126. (c) Cvitas, T.; Klasinc, L.; Kovac, B.; McDiarmid, R. *J. Chem. Phys.* **1983**, *79*, 1565.

(18) Kimura, K.; Katsumata, S.; Achiba, Y.; Yamazaki, T.; Iwata, S. *Handbook of He I Photoelectron Spectra of Fundamental Organic Molecules*; Japan Scientific Press: Tokyo, 1981.

(19) Bastide, J.; Maier, J. P. *Chem. Phys.* **1976**, *12*, 177.

(20) (a) Eland, J. H. D. *Philos. Trans. R. Soc. London, Ser. A* **1970**, *268*, 87. (b) Cradock, S.; Ebsworth, E. A. V.; Murdoch, J. D. *J. Chem. Soc., Faraday Trans. 2* **1972**, *68*, 86. (c) Cvitas, T.; Klasinc, L. *J. Chem. Soc., Faraday Trans. 2* **1976**, *72*, 1240.

(21) Lee, T. H.; Colton, R. J.; White, M. G.; Rabalais, J. W. *J. Am. Chem. Soc.* **1975**, *97*, 4845.

(22) (a) Čermák, V. *J. Electron. Spectrosc. Relat. Phenom.* **1976**, *9*, 419. (b) Brion, C. E.; Yee, D. S. C. *J. Electron. Spectrosc. Relat. Phenom.* **1977**, *12*, 77.

(23) Hotop, H.; Kolb, E.; Lorenzen, J. *J. Electron. Spectrosc. Relat. Phenom.* **1979**, *16*, 213.

(24) Wentrup, C.; Gerecht, B.; Briehl, H. *Angew. Chem., Int. Ed. Engl.* **1979**, *18*, 467.

(25) (a) Gunther, P.; Meyer, R. *Z. Elektrochem.* **1935**, *41*, 541. (b) Krakow, B.; Lord, R. C.; Neeby, G. O. *J. Mol. Spectrosc.* **1968**, *27*, 148.

(26) Claisen, L.; Zedel, W. *Chem. Ber.* **1891**, *24*, 140.

(27) Mitsuke, K.; Takami, T.; Ohno, K. *J. Chem. Phys.* **1989**, *91*, 1618.

(28) Gardner, J. L.; Samson, J. A. R. *J. Electron. Spectrosc. Relat. Phenom.* **1976**, *8*, 469.

(29) (a) Rothe, E. W.; Neynaber, R. H.; Trajillo, S. M. *J. Chem. Phys.* **1965**, *42*, 3310. (b) Niehaus, A. *Adv. Chem. Phys.* **1981**, *45*, 399. (c) Hotop, H. *Radiat. Res.* **1974**, *59*, 379. (d) Haberland, H.; Lee, Y. T.; Siska, P. E. *Adv. Chem. Phys.* **1981**, *45*, 487.

(30) (a) Teffo, J. L.; Chédin, A. *J. Mol. Spectrosc.* **1989**, *135*, 389. (b) Bunker, P. R.; Landsberg, B. M.; Winnewisser, B. P. *J. Mol. Spectrosc.* **1979**, *74*, 9. (c) Winnewisser, B. P. *J. Mol. Spectrosc.* **1980**, *82*, 220.

(31) Boys, S. F.; Bernardi, F. *Mol. Phys.* **1970**, *10*, 553.

(32) Frisch, M. J.; Trucks, G. W.; Schlegel, H. B.; Gill, P. M. W.; Johnson, B. G.; Robb, M. A.; Cheeseman, J. R.; Keith, T.; Petersson, G. A.; Montgomery, J. A.; Raghavachari, K.; Al-Laham, M. A.; Zakrzewski, V. G.; Ortiz, J. V.; Foresman, J. B.; Cioslowski, J.; Stefanov, B. B.; Nanayakkara, A.; Challacombe, M.; Peng, C. Y.; Ayala, P. Y.; Chen, W.; Wong, M. W.; Andres, J. L.; Replogle, E. S.; Gomperts, R.; Martin, R. L.; Fox, D. J.; Binkley, J. S.; Defrees, D. J.; Baker, J.; Stewart, J. P.; Head-Gordon, M.; Gonzalez, C.; Pople, J. A. *Gaussian 94*, revision C.3; Gaussian, Inc.: Pittsburgh, PA, 1995.

(33) von Niessen, W.; Schirmer, J.; Cederbaum, L. S. *Comput. Phys. Rep.* **1984**, *1*, 57.

(34) Åsbrink, L.; Fridh, C.; Lindholm, E. *Chem. Phys. Lett.* **1977**, *52*, 69. The HAM/3 program is available from the Quantum Chemistry Program Exchange, Indiana University, Bloomington, IN (D. P. Chong, QCMP005, 1985).

(35) Chong, D. P. *Theor. Chim. Acta* **1979**, *51*, 55.

(36) Zeiss, G. D.; Chong, D. P. *J. Electron. Spectrosc. Relat. Phenom.* **1980**, *18*, 279.

(37) Pasinszki, T.; Kishimoto, N.; Ohno, K. Manuscript in preparation.

(38) Ohno, K.; Takami, T.; Mitsuke, K.; Ishida, T. *J. Chem. Phys.* **1991**, *94*, 2675.

(39) Calculated total atomic charges (natural population analysis using the QCISD density; calculations were done at the optimized QCISD geometries of molecules). N(1)N(2)O: N(1), −0.06; N(2), +0.40; O, −0.34. HCNO: H, +0.23; C, −0.01; N, +0.19; O, −0.41. HN(1)N(2)N(3): H, +0.34; N(1), −0.53; N(2), +0.23; N(3), −0.04.

(40) Calculated structure and rotational constants of HCNOLi π-complex, HCNOLi(II), using the B3LYP/6-311++G** method: CH = 1.088 Å, CN = 1.261 Å, NO = 1.301 Å, LiC = 2.032 Å, LiO = 1.823 Å, ONC = 131.5°, NCH = 118.2°; total energy = −176.179464 au; bonding energy = 157.3 kJ/mol; A = 25.1756, B = 11.8161, C = 8.0417 GHz.

(41) Calculated structure and energy of HCNOLi(I) at the B3LYP/6-311++G** level: CH = 1.091 Å, CN = 1.242 Å, NO = 1.321 Å, LiO = 1.615 Å, HCN = 119.2°, CNO = 129.3°, NOLi = 172.2°; total energy = −176.163340 au; bonding energy = 115.0 kJ/mol; barrier to isomerization = 5.6 kJ/mol.

(42) Schulz, C. P.; Hertel, I. V. Solvated Atoms in Polar Solvents. In *Clusters of Atoms and Molecules II*; Haberland, H., Ed.; Springer-Verlag: Berlin-Heidelberg, 1994; pp 7−18.